Mineralogical Magazine (2022), **86**, 397–404
doi:10.1180/mgm.2022.37

CAMBRIDGE UNIVERSITY PRESS

Article

Flaggite, $Pb_4Cu_4^{2+}Te_2^{6+}(SO_4)_2O_{11}(OH)_2(H_2O)$, a new mineral with stair-step-like HCP layers from Tombstone, Arizona, USA

Anthony R. Kampf[1]*, Stuart J. Mills[2], Aaron J. Celestian[1], Chi Ma[3], Hexiong Yang[4] and Brent Thorne[5]

[1]Mineral Sciences Department, Natural History Museum of Los Angeles County, 900 Exposition Boulevard, Los Angeles, CA 90007, USA; [2]Geosciences, Museums Victoria, GPO Box 666, Melbourne 3001, Victoria, Australia; [3]Division of Geological and Planetary Sciences, California Institute of Technology, 1200 East California Boulevard, Pasadena, California 91125, USA; [4]Department of Geosciences, University of Arizona, 1040 E. 4th Street, Tucson, AZ 85721, USA; and [5]Independent Researcher, Bountiful, UT 84010, USA

Abstract

The new mineral flaggite (IMA2021-044), $Pb_4Cu_4^{2+}Te_2^{6+}(SO_4)_2O_{11}(OH)_2(H_2O)$, occurs at the Grand Central mine in the Tombstone district, Cochise County, Arizona, USA, in cavities in quartz matrix in association with alunite, backite, cerussite, jarosite and rodalquilarite. Flaggite crystals are lime-green to yellow-green tablets, up to 0.5 mm across. The mineral has a very pale green streak and adamantine lustre. It is brittle with irregular fracture and a Mohs hardness of ~3. It has one excellent cleavage on {010}. The calculated density is 6.137 g cm^{-3}. Optically, the mineral is biaxial (+) with $\alpha = 1.95(1)$, $\beta = 1.96(1)$, $\gamma = 2.00(1)$ (white light); $2V = 54(2)°$; pleochroism: X green, Y light yellow green, Z nearly colourless; $X > Y > Z$. The Raman spectrum exhibits bands consistent with TeO_6 and SO_4. Electron microprobe analysis provided the empirical formula $Pb_{3.88}Cu_{3.89}^{2+}Te_{2.08}^{6+}(SO_4)_2O_{11}(OH)_2(H_2O)$ (–0.03 H). Flaggite is triclinic, $P\bar{1}$, $a = 9.5610(2)$, $b = 9.9755(2)$, $c = 10.4449(3)$ Å, $\alpha = 74.884(1)$, $\beta = 89.994(1)$, $\gamma = 78.219(1)°$, $V = 939.97(4)$ Å^3 and $Z = 2$. The structure of flaggite ($R_1 = 0.0342$ for 5936 $I > 2\sigma I$) contains hexagonal-close-packed, stair-step-like layers comprising TeO_6 octahedra and Jahn-Teller distorted CuO_6 octahedra. The layers in the structure of flaggite are very similar to those in bairdite, timroseite and paratimroseite.

Keywords: flaggite, new mineral, tellurate, crystal structure, Raman spectroscopy, HCP layers, bairdite, timroseite, paratimroseite, Tombstone, Arizona, USA

(Received 28 February 2022; accepted 29 March 2022; Accepted Manuscript published online: 18 April 2022; Associate Editor: Irina O Galuskina)

Introduction

Despite the rich chemical and structural diversity of tellurium oxysalt minerals (Christy *et al.*, 2016a), relatively few contain additional sulfate anions. This seems surprising considering the prevalence of sulfides in the ore deposits in which many tellurium oxysalt minerals form from the weathering of primary minerals, such as hessite, altaite or native Te (e.g. Mills *et al.*, 2014; Missen *et al.*, 2020, 2022a) in association with sulfides, such as galena and chalcopyrite. In these environments, sulfur is usually not incorporated into the structures of tellurium oxysalts. Here, we report the new mineral flaggite, which is only the 15th tellurium oxysalt mineral to contain essential sulfate (or thiosulfate) within its structure (Christy *et al.*, 2016b; Missen *et al.*, 2022b). Bairdite, $Pb_2Cu_4^{2+}Te_2^{6+}O_{10}(OH)_2(SO_4)(H_2O)$ (Kampf *et al.*, 2013) and tombstoneite, $(Ca_{0.5}Pb_{0.5})Pb_3Cu_6^{2+}Te_2^{6+}O_6(Te^{4+}O_3)_6(Se^{4+}O_3)_2(SO_4)_2{\cdot}3H_2O$ (Kampf *et al.*, 2021b), are the only other minerals that contain essential Pb, Cu, Te and S, all common elements found in tellurium ore deposits.

Flaggite is named in honour of Arthur L. Flagg (1883–1961). Professionally, Mr. Flagg was a mining engineer; however, first and foremost, mineralogy was his passionate avocation. During his studies at Brown University, Flagg was assigned to work with the USGS on geological quadrangle surveys in central Arizona. He fell in love with the state (at that time still a territory) and, following his graduation in 1906, he moved there to begin a career in mining, geology and mineralogy that spanned more than 55 years. His vast geological and mining experience focusing on Arizona, led to his being regarded as an expert on Arizona mineral resources. Flagg was particularly known as a proponent of educating the public about minerals and promoting the mineral collecting hobby. He was a founder, active member and president of several mining and mineralogical groups including the Mineralogical Society of Arizona, the Small Mine Operators Association, the American Federation of Mineralogical Societies, and the Rocky Mountain Federation of Mineralogical Societies. He lectured and wrote extensively, publishing two books for mineral collectors, *Rockhounds and Arizona Minerals* (1944) and *Mineralogical Journeys in Arizona* (1958), several articles on minerals for *Arizona Highways* and *Rocks & Minerals*, and papers in the *Bulletin of the American Institute of Mining Engineers*. In 1949, Flagg was hired by the Arizona Department of Mineral Resources to be the first curator of the Arizona Mineral Museum (now the Arizona Mining and Mineral Museum) in Phoenix, Arizona, a position he held until his death in 1961. The naming of this mineral for Arthur L. Flagg is particularly appropriate in recognition of the inspiration he provided to generations of future collectors and Earth scientists.

***Author for correspondence:** Anthony R. Kampf, Email: akampf@nhm.org
Cite this article: Kampf A.R., Mills S.J., Celestian A.J., Ma C., Yang H. and Thorne B. (2022) Flaggite, $Pb_4Cu_4^{2+}Te_2^{6+}(SO_4)_2O_{11}(OH)_2(H_2O)$, a new mineral with stair-step-like HCP layers from Tombstone, Arizona, USA. *Mineralogical Magazine* **86**, 397–404. https://doi.org/10.1180/mgm.2022.37

The new mineral and name (symbol Flg) were approved by the Commission on New Minerals, Nomenclature and Classification of the International Mineralogical Association (IMA2021-044, Kampf *et al.*, 2021a). The description is based on one holotype and two cotype specimens deposited in the collections of the Natural History Museum of Los Angeles County, Los Angeles, California, USA; catalogue numbers 64499 (cotype), 64500 (cotype) and 76143 (holotype). Specimens 64499 and 64500 are also cotypes for backite.

Occurrence

Flaggite occurs at the Grand Central mine (coordinates: 31.70250, –110.06194) in the Tombstone district, Cochise County, Arizona, USA, ~1 km south of the town of Tombstone. The three type specimens were originally collected by Sidney A. Williams and were obtained by one of the authors (BT) from Excalibur Minerals. The Grand Central mine exploits a Ag–Au–Pb–Cu–Zn deposit in which the ore, consisting principally of oxidised Ag- and Au-rich galena, occurs in faulted and fractured portions of a large dyke hosted by the Bisbee Group limestone. A good description of the history, geology and mineralogy of the Tombstone district was provided by Williams (1980). Flaggite occurs in cavities in quartz matrix in association with alunite, backite, cerussite, jarosite and rodalquilarite.

Physical and optical properties

Flaggite crystals are tablets (Fig. 1) up to ~0.5 mm across and up to 0.2 mm thick (Fig. 1). On the cotype specimens, flaggite occurs as thin plates grouped in rosettes up to 0.1 mm in diameter (Fig. 2). Tablets are probably flattened on {010} based on the structure, but crystals are too small and irregular to measure forms. Twinning is ubiquitous, by 180° rotation on [001]. Crystals are lime green to yellow green and transparent with adamantine lustre. The streak is very pale green. No fluorescence was observed in either longwave or shortwave ultraviolet illumination. The Mohs hardness is ~3 based upon scratch tests. Crystals are brittle with irregular fracture. There is one excellent cleavage on {010}. The density could not be measured because it exceeds that of available density liquids and there is an insufficient quantity for physical measurement. The calculated density based on the empirical formula and unit-cell parameters obtained from single-crystal X-ray diffraction data is 6.137 g cm^{-3} and that for the ideal formula is 6.212 g cm^{-3}. At room temperature, flaggite decomposes in dilute HCl, losing birefringence and becoming white and translucent.

Optically, flaggite is biaxial (+), with $\alpha = 1.95(1)$, $\beta = 1.96(1)$ and $\gamma = 2.00(1)$ measured in white light. The 2V measured using extinction data with *EXCALIBR* (Gunter *et al.*, 2004) is 54(2)° and the calculated 2V is 54.0°. The dispersion could not be observed and the optical orientation was not determined because of the difficulty in determining the orientation of the irregularly shaped crystals. The pleochroism is *X* green, *Y* light yellow green and *Z* nearly colourless; $X > Y > Z$. The Gladstone–Dale compatibility index $1 - (K_P/K_C)$ for the empirical formula is –0.012 and that for the ideal formula is –0.003, in both cases in the superior range (Mandarino, 2007).

Raman Spectroscopy

Raman spectroscopy was conducted on a Horiba XploRA PLUS using a 532 nm diode laser, 50 μm slit, 2400 gr/mm diffraction grating and a 100× (0.9 NA) objective. Selected regions of the spectrum recorded perpendicular to the {010} cleavage are shown in Fig. 3. The Raman spectrum is very complex due to the low symmetry of the structure and the large number of independent cation sites. The assignments for the TeO_6 ν_1 symmetric stretching and SO_4 ν_1 symmetric stretching are straightforward and are diagnostic for this mineral, and they have been labelled in Fig. 3, as has the weak band at 1092 cm^{-1} and the broad associated features, which are related to SO_4 ν_3 antisymmetric stretching. Bairdite on the other hand has only a single SO_4 ν_1 symmetric stretching band at 977 cm^{-1} and the TeO_6 ν_1 symmetric stretching band is located at 721 cm^{-1} (Kampf *et al.*, 2013). We do not feel confident in assigning modes to specific bands in the 650 to 300 cm^{-1} range; however, these all are likely to be due to CuO_6 and TeO_6 stretching, as well as SO_4, CuO_6, and TeO_6 bending modes. The very weak band at 1425 cm^{-1} could be due to H_2O bending. The spectrum is featureless between the 1425 cm^{-1} band and the OH stretching region.

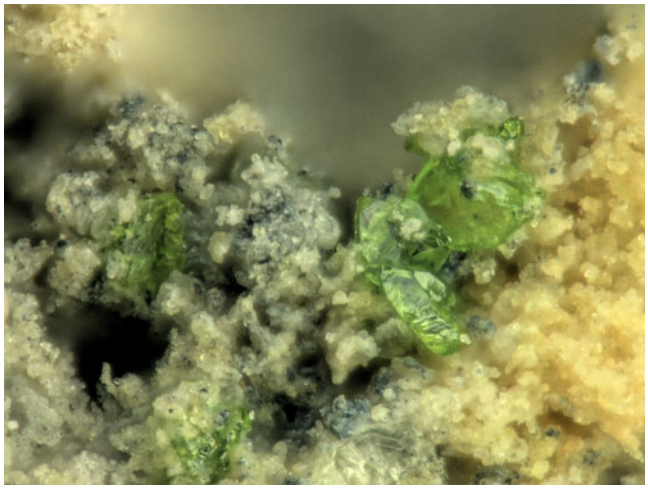

Fig. 1. Flaggite tablets (green) with alunite (yellow) on quartz; holotype specimen #76143; field of view 0.45 mm across.

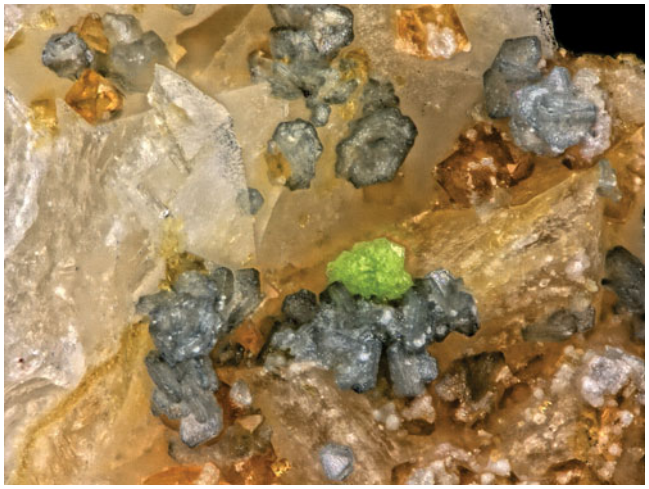

Fig. 2. Rosette of flaggite plates (green) with backite (grey) and jarosite (yellow orange) on quartz; cotype specimen #64499; field of view 0.56 mm across.

https://doi.org/10.1180/mgm.2022.37 Published online by Cambridge University Press

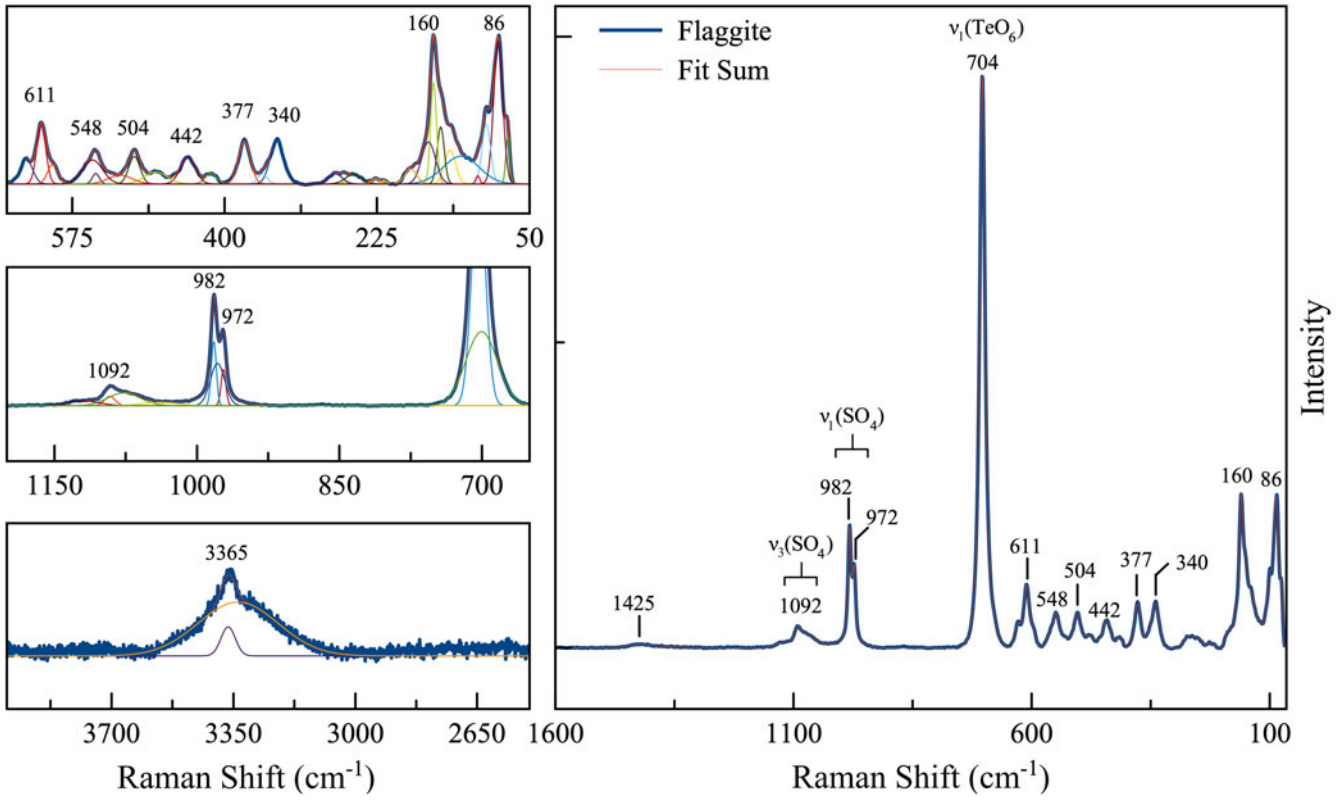

Fig. 3. Selected regions of the Raman spectrum of flaggite recorded perpendicular to the {010} cleavage with a 532 nm laser. Top left: region for CuO_6 and TeO_6 stretching, as well as SO_4, CuO_6, and TeO_6 bending modes. Left middle: region for SO_4 and TeO_6 stretching modes. Left bottom: region for OH stretching modes. Right: overview of Raman spectrum.

Chemical composition

Analyses (8 points) were performed at Caltech on a JEOL 8200 electron microprobe in WDS mode. Analytical conditions were 15 kV accelerating voltage, 10 nA beam current and 2 μm beam diameter. Insufficient material is available for CHN analysis; however, the fully ordered structure unambiguously established the quantitative content of H_2O. Analytical data are given in Table 1. The empirical formula based on S = 2 and O = 22 atoms per formula unit is $Pb_{3.88}Cu^{2+}_{3.89}Te^{6+}_{2.08}(SO_4)_2O_{11}(OH)_2(H_2O)$ (–0.03 H for charge balance). The ideal formula is $Pb_4Cu^{2+}_4Te^{6+}_2(SO_4)_2O_{11}(OH)_2(H_2O)$, which requires PbO 50.78, CuO 18.10, TeO_3 19.97, SO_3 9.11, H_2O 2.05, total 100 wt.%.

X-ray crystallography and structure refinement

Powder X-ray diffraction was done using a Rigaku R-Axis Rapid II curved-imaging-plate microdiffractometer, with monochromatised Mo*K*α radiation. A Gandolfi-like motion on the φ and ω

Table 1. Chemical composition (in wt.%) for flaggite.

Constituent	Mean	Range	S.D.	Standard
PbO	50.18	48.76–51.28	0.74	PbS
CuO	17.91	17.55–18.30	0.23	Cu metal
TeO_3	21.17	20.97–21.37	0.15	Te metal
SO_3	9.27	9.11–9.53	0.14	anhydrite
H_2O*	2.07			
Total	100.60			

*Based upon the crystal structure with S = 2 and O = 22 atoms per formula unit.
S.D. – standard deviation

Table 2. Data collection and structure refinement details for flaggite.*

Crystal data	
Structural formula	$Pb_4Cu^{2+}_4Te^{6+}_2(SO_4)_2O_{11}(OH)_2(H_2O)$ [including unlocated H atoms]
Crystal size (μm)	60 × 40 × 30
Space group	*P*1 (#1)
Unit cell dimensions	*a* = 9.5610(2) Å
	b = 9.9755(2) Å
	c = 10.4449(3) Å
	α = 74.8840(10)°
	β= 89.9940(10)°
	γ = 78.2190(10)°
V	939.97(4) Å^3
Z	2
Density (for above formula)	6.212 g cm^{-3}
Absorption coefficient	43.495 mm^{-1}
Data collection	
Diffractometer	Bruker APEX2 CCD
X-ray radiation / power	Mo*K*α (λ = 0.71073 Å)/50 kV, 40 mA
Temperature	293(2) K
F(000)	1520
θ range	2.18 to 33.15°
Refls collected / unique	73177 / 7135; R_{int} = 0.0603
Reflections with $I > 2\sigma I$	5936
Completeness to θ = 33.15°	99.6%
Index ranges	$-14 \le h \le 14$, $-15 \le k \le 15$, $-8 \le l \le 15$
Refinement	
Refinement method	Full-matrix least-squares on F^2
Parameters / restraints	474 / 3
GoF	0.997
Final *R* indices [$I_o > 2\sigma I$]	R_1 = 0.0339, wR_2 = 0.0576
R indices (all data)	R_1 = 0.0454, wR_2 = 0.0597
Abs. structure parameter	0.432(10)
Largest diff. peak / hole	+6.46 / –3.70 e^-/Å^3

*$R_{int} = \Sigma|F_o^2 - F_o^2(\text{mean})|/\Sigma[F_o^2]$. GoF = $S = \{\Sigma[w(F_o^2 - F_c^2)^2]/(n-p)\}^{½}$. $R_1 = \Sigma||F_o| - |F_c||/\Sigma|F_o|$. $wR_2 = \{\Sigma[w(F_o^2 - F_c^2)^2]/\Sigma[w(F_o^2)^2]\}^{½}$; $w = 1/[\sigma^2(F_o^2) + (aP)^2 + bP]$ where *a* is 0.0241, *b* is 0 and *P* is $[2F_c^2 + \text{Max}(F_o^2, 0)]/3$.

https://doi.org/10.1180/mgm.2022.37 Published online by Cambridge University Press

Table 3. Atom coordinates and displacement parameters (Å^2) for flaggite.

	x/a	*y/b*	*z/c*	U_{eq}	U^{11}	U^{22}	U^{33}	U^{23}	U^{13}	U^{12}
Pb1	0.87241(5)	0.30643(5)	0.55377(5)	0.01142(11)	0.0121(3)	0.0093(2)	0.0114(2)	−0.00128(18)	−0.00414(18)	−0.0009(2)
Pb2	0.87875(6)	0.31213(5)	0.06558(5)	0.01364(11)	0.0147(3)	0.0108(3)	0.0132(2)	−0.00184(18)	−0.00206(19)	0.0007(2)
Pb3	0.40898(6)	0.86870(5)	0.88272(5)	0.01360(11)	0.0116(3)	0.0151(2)	0.0117(2)	−0.00045(19)	0.00025(18)	−0.0012(2)
Pb4	0.36983(6)	0.30771(5)	0.72037(5)	0.01402(12)	0.0123(3)	0.0126(3)	0.0142(2)	−0.00151(19)	0.00050(19)	0.0014(2)
Pb5	0.91014(6)	0.86826(5)	0.11771(5)	0.01350(11)	0.0113(3)	0.0153(2)	0.0149(2)	−0.00681(19)	0.00018(18)	−0.0017(2)
Pb6	0.95621(6)	0.86228(5)	0.69735(5)	0.01367(10)	0.0112(3)	0.0125(2)	0.0162(2)	−0.00253(18)	0.00135(18)	−0.00177(19)
Pb7	0.45647(6)	0.86471(5)	0.30376(5)	0.01423(10)	0.0124(3)	0.0132(2)	0.0169(2)	−0.00463(18)	−0.00219(18)	−0.00172(19)
Pb8	0.38078(6)	0.31000(5)	0.21857(6)	0.01595(12)	0.0159(3)	0.0123(3)	0.0177(2)	−0.00214(19)	0.0023(2)	−0.0010(2)
Cu1	0.29179(17)	0.66710(17)	0.66720(15)	0.0069(3)	0.0044(9)	0.0100(8)	0.0051(7)	−0.0001(6)	−0.0015(6)	−0.0015(7)
Cu2	0.03033(17)	0.49656(17)	0.72879(14)	0.0065(3)	0.0022(8)	0.0124(8)	0.0049(6)	−0.0017(6)	0.0005(5)	−0.0019(6)
Cu3	0.03618(17)	0.50302(17)	0.22909(14)	0.0065(3)	0.0014(8)	0.0138(8)	0.0051(6)	−0.0037(6)	0.0000(5)	−0.0019(6)
Cu4	0.28755(17)	0.66700(17)	0.16667(15)	0.0072(3)	0.0043(9)	0.0086(8)	0.0079(7)	−0.0001(6)	−0.0015(6)	−0.0026(7)
Cu5	0.53018(18)	0.49658(17)	0.45738(14)	0.0071(3)	0.0048(8)	0.0110(8)	0.0037(6)	0.0006(5)	0.0013(5)	−0.0011(6)
Cu6	0.79209(17)	0.66747(17)	0.43404(15)	0.0062(3)	0.0009(8)	0.0126(8)	0.0040(7)	−0.0001(6)	−0.0002(5)	−0.0012(7)
Cu7	0.53599(17)	0.50435(17)	0.95280(14)	0.0066(3)	0.0038(8)	0.0104(8)	0.0047(6)	−0.0001(5)	0.0010(5)	−0.0019(6)
Cu8	0.78685(17)	0.66801(17)	0.93158(15)	0.0074(3)	0.0024(8)	0.0106(8)	0.0092(7)	−0.0016(6)	0.0028(6)	−0.0026(7)
Te1	0.15891(9)	0.57662(9)	0.45645(9)	0.00454(15)	0.0015(4)	0.0089(4)	0.0029(3)	−0.0006(3)	0.0009(3)	−0.0015(3)
Te2	0.65927(10)	0.57864(9)	0.68863(9)	0.00523(15)	0.0023(4)	0.0091(4)	0.0040(3)	−0.0008(3)	0.0010(3)	−0.0017(3)
Te3	0.16125(9)	0.57737(9)	0.94782(9)	0.00403(14)	0.0007(4)	0.0065(3)	0.0041(3)	0.0004(3)	0.0003(3)	−0.0011(3)
Te4	0.66093(9)	0.57554(9)	0.19773(9)	0.00367(14)	0.0012(4)	0.0070(4)	0.0020(3)	0.0002(3)	0.0006(2)	−0.0011(3)
S1	0.0688(3)	0.1290(3)	0.8599(3)	0.0082(6)	0.0063(16)	0.0078(15)	0.0086(13)	0.0000(11)	0.0031(11)	−0.0003(12)
S2	0.0810(4)	0.1207(4)	0.3560(3)	0.0120(7)	0.0046(16)	0.0140(17)	0.0136(15)	0.0011(12)	0.0004(12)	0.0003(13)
S3	0.5750(4)	0.1219(3)	0.5166(3)	0.0121(7)	0.0168(19)	0.0090(16)	0.0094(14)	−0.0004(12)	−0.0004(12)	−0.0027(14)
S4	0.5743(4)	0.1284(3)	0.0095(3)	0.0112(7)	0.0151(19)	0.0084(16)	0.0102(14)	−0.0031(12)	−0.0003(12)	−0.0018(13)
O1	0.9971(12)	0.0762(10)	0.7660(10)	0.025(2)	0.036(7)	0.015(5)	0.025(5)	−0.008(4)	−0.011(5)	−0.003(5)
O2	0.0555(11)	0.0497(10)	0.9981(9)	0.015(2)	0.016(5)	0.015(5)	0.011(4)	0.003(4)	0.005(4)	−0.006(4)
O3	0.9970(10)	0.2786(9)	0.8428(9)	0.013(2)	0.013(5)	0.002(4)	0.020(5)	0.005(3)	0.001(4)	−0.001(4)
O4	0.2230(11)	0.1170(11)	0.8349(10)	0.025(3)	0.012(6)	0.024(6)	0.031(6)	0.009(4)	0.002(4)	−0.008(5)
O5	0.9886(12)	0.2625(10)	0.3190(10)	0.027(3)	0.023(6)	0.013(5)	0.033(6)	0.007(4)	0.017(4)	0.009(4)
O6	0.2281(11)	0.1229(12)	0.3156(10)	0.025(3)	0.010(6)	0.033(6)	0.027(6)	0.006(5)	0.006(4)	−0.013(5)
O7	0.0768(11)	0.0631(11)	0.5014(9)	0.022(2)	0.020(6)	0.029(6)	0.009(4)	0.006(4)	0.006(4)	−0.003(5)
O8	0.0184(13)	0.0294(13)	0.2901(11)	0.041(3)	0.034(8)	0.071(9)	0.033(6)	−0.026(6)	0.010(5)	−0.031(7)
O9	0.5777(12)	0.0647(13)	0.3993(11)	0.031(3)	0.016(6)	0.045(7)	0.035(6)	−0.024(6)	−0.012(5)	0.003(5)
O10	0.5157(11)	0.0282(10)	0.6280(10)	0.022(2)	0.021(6)	0.015(5)	0.026(5)	0.009(4)	−0.006(4)	−0.012(4)
O11	0.4834(10)	0.2668(9)	0.4806(9)	0.0125(19)	0.008(5)	0.007(4)	0.020(5)	−0.001(3)	−0.005(3)	0.003(4)
O12	0.7247(12)	0.1217(11)	0.5575(11)	0.024(2)	0.022(6)	0.018(6)	0.031(6)	−0.002(4)	−0.002(5)	−0.009(5)
O13	0.5023(12)	0.0754(10)	0.1301(10)	0.026(3)	0.037(7)	0.029(6)	0.026(5)	−0.016(5)	0.020(5)	−0.026(5)
O14	0.5060(11)	0.2783(10)	0.9508(10)	0.020(2)	0.022(6)	0.006(5)	0.029(5)	−0.002(4)	−0.010(4)	0.004(4)
O15	0.5588(11)	0.0455(11)	0.9145(9)	0.017(2)	0.019(6)	0.021(5)	0.015(5)	−0.006(4)	−0.004(4)	−0.012(4)
O16	0.7288(12)	0.1101(11)	0.0435(11)	0.028(3)	0.022(7)	0.015(6)	0.041(7)	−0.009(5)	0.002(5)	0.008(5)
O17	0.1034(10)	0.6936(10)	0.5733(8)	0.0104(18)						
O18	0.1295(10)	0.4125(9)	0.5867(8)	0.0105(18)						
O19	0.9750(10)	0.6062(9)	0.3653(8)	0.0097(18)						
O20	0.2214(11)	0.4856(10)	0.3179(9)	0.016(2)						
O21	0.3503(9)	0.5420(9)	0.5376(8)	0.0067(17)						
O22	0.1971(11)	0.7538(10)	0.3291(9)	0.016(2)						
O23	0.6301(10)	0.4129(9)	0.6443(8)	0.0106(18)						
O24	0.6027(9)	0.6925(9)	0.5117(8)	0.0053(16)						
O25	0.7253(9)	0.4948(8)	0.8704(7)	0.0080(17)						
O26	0.4775(10)	0.6099(9)	0.7658(8)	0.0099(18)						
O27	0.8488(9)	0.5481(9)	0.6254(8)	0.0078(17)						
O28	0.6948(10)	0.7556(9)	0.7263(8)	0.0139(19)						
O29	0.1248(10)	0.4209(9)	0.0864(8)	0.0090(18)						
O30	0.1042(10)	0.6964(9)	0.0652(8)	0.0089(18)						
O31	0.3514(10)	0.5393(9)	0.0285(8)	0.0101(18)						
O32	0.2128(10)	0.4632(9)	0.8251(8)	0.0098(18)						
O33	0.1951(10)	0.7436(10)	0.8136(8)	0.0126(19)						
O34	0.9710(10)	0.6124(9)	0.8599(8)	0.0081(17)						
O35	0.7103(9)	0.4608(8)	0.3746(7)	0.0067(16)						
O36	0.8504(9)	0.5376(9)	0.1368(8)	0.0069(17)						
O37	0.6231(10)	0.4191(9)	0.1373(8)	0.0097(18)						
O38	0.6986(9)	0.7381(8)	0.2499(7)	0.0047(16)						
O39	0.6046(9)	0.6968(9)	0.0202(7)	0.0047(16)						
O40	0.4710(9)	0.6099(9)	0.2681(8)	0.0061(17)						
O41	0.8286(10)	0.8571(9)	0.9170(8)	0.0113(19)						
O42	0.3294(10)	0.8650(10)	0.0870(9)	0.014(2)						
O43	0.8310(11)	0.8812(10)	0.4282(9)	0.021(2)						
O44	0.3329(12)	0.8783(11)	0.5622(10)	0.025(2)						

https://doi.org/10.1180/mgm.2022.37 Published online by Cambridge University Press

Table 4. Selected interatomic distances (Å) in flaggite.

Pb1–O35	2.408(8)	Pb2–O36	2.512(8)	Pb3–O42	2.259(9)	Pb4–O32	2.406(8)
Pb1–O12	2.533(10)	Pb2–O25	2.570(8)	Pb3–O39	2.430(8)	Pb4–O18	2.565(9)
Pb1–O23	2.629(9)	Pb2–O37	2.650(9)	Pb3–O15	2.571(10)	Pb4–O21	2.577(8)
Pb1–O27	2.672(8)	Pb2–O3	2.656(9)	Pb3–O4	2.665(11)	Pb4–O4	2.632(10)
Pb1–O5	2.793(10)	Pb2–O5	2.731(11)	Pb3–O33	2.788(9)	Pb4–O14	2.655(10)
Pb1–O1	2.799(10)	Pb2–O16	2.756(12)	Pb3–O10	3.018(10)	Pb4–O11	2.823(9)
Pb1–O18	2.921(9)	Pb2–O29	2.815(9)	Pb3–O26	3.088(9)	Pb4–O23	2.925(9)
Pb1–O7	2.961(11)	Pb2–O2	3.060(10)	Pb3–O28	3.334(9)	Pb4–O15	3.086(10)
Pb1–O3	3.169(9)	Pb2–O8	3.201(13)	Pb3–O31	3.398(9)	Pb4–O10	3.235(10)
Pb1–O19	3.451(9)	<Pb2–O>	2.772	Pb3–O44	3.399(10)	<Pb4–O>	2.767
<Pb1–O>	2.834			<Pb3–O>	2.895		
Pb5–O41	2.274(8)	Pb6–O33	2.498(9)	Pb7–O13	2.508(10)	Pb8–O20	2.515(9)
Pb5–O30	2.424(9)	Pb6–O1	2.522(10)	Pb7–O38	2.539(8)	Pb8–O31	2.573(9)
Pb5–O2	2.572(9)	Pb6–O17	2.581(9)	Pb7–O42	2.569(9)	Pb8–O6	2.601(10)
Pb5–O16	2.597(10)	Pb6–O41	2.591(8)	Pb7–O24	2.588(8)	Pb8–O29	2.686(9)
Pb5–O38	2.796(8)	Pb6–O34	2.601(8)	Pb7–O40	2.639(8)	Pb8–O13	2.774(10)
Pb5–O8	3.014(11)	Pb6–O7	2.888(10)	Pb7–O9	2.881(11)	Pb8–O37	2.797(9)
Pb5–O19	3.117(8)	Pb6–O28	2.896(9)	Pb7–O22	2.900(10)	Pb8–O11	2.802(9)
Pb5–O22	3.334(10)	Pb6–O43	3.000(10)	Pb7–O44	2.971(10)	Pb8–O9	2.968(11)
Pb5–O43	3.360(9)	Pb6–O12	3.069(10)	Pb7–O6	3.047(11)	Pb8–O14	3.108(10)
Pb5–O36	3.416(8)	<Pb6–O>	2.738	<Pb7–O>	2.738	Pb8–O40	3.439(8)
<Pb5–O>	2.890					<Pb8–O>	2.826
Cu1–O26	1.954(9)	Cu2–O32	1.937(9)	Cu3–O36	1.944(9)	Cu4–O40	1.950(9)
Cu1–O17	1.987(10)	Cu2–O27	1.946(9)	Cu3–O20	1.954(10)	Cu4–O30	1.977(9)
Cu1–O33	2.024(9)	Cu2–O34	2.022(8)	Cu3–O19	1.986(9)	Cu4–O42	2.054(9)
Cu1–O21	2.073(8)	Cu2–O18	2.032(8)	Cu3–O29	1.991(8)	Cu4–O31	2.173(8)
Cu1–O44	2.220(11)	Cu2–O3	2.275(9)	Cu3–O30	2.422(9)	Cu4–O22	2.199(9)
Cu1–O32	2.511(9)	Cu2–O17	2.426(9)	Cu3–O5	2.473(10)	Cu4–O20	2.268(9)
<Cu1–O_{eq}>	2.010	<Cu2–O_{eq}>	1.984	<Cu3–O_{eq}>	1.969	<Cu4–O_{eq}>	2.039
<Cu1–O_{ap}>	2.366	<Cu2–O_{ap}>	2.351	<Cu3–O_{ap}>	2.448	<Cu4–O_{ap}>	2.234
Cu5–O21	1.935(9)	Cu6–O19	1.934(9)	Cu7–O31	1.937(9)	Cu8–O34	1.945(9)
Cu5–O35	1.936(8)	Cu6–O24	1.980(9)	Cu7–O26	1.981(9)	Cu8–O41	1.975(9)
Cu5–O40	2.020(8)	Cu6–O38	2.008(7)	Cu7–O37	1.997(8)	Cu8–O39	1.978(8)
Cu5–O23	2.061(8)	Cu6–O27	2.050(8)	Cu7–O25	2.000(8)	Cu8–O25	2.175(8)
Cu5–O11	2.375(9)	Cu6–O43	2.224(10)	Cu7–O14	2.336(10)	Cu8–O28	2.201(9)
Cu5–O24	2.399(9)	Cu6–O35	2.564(8)	Cu7–O39	2.415(8)	Cu8–O36	2.209(8)
<Cu5–O_{eq}>	1.988	<Cu6–O_{eq}>	1.993	<Cu7–O_{eq}>	1.979	<Cu8–O_{eq}>	2.018
<Cu5–O_{ap}>	2.387	<Cu6–O_{ap}>	2.394	<Cu7–O_{ap}>	2.376	<Cu8–O_{ap}>	2.205
Te1–O17	1.903(9)	Te2–O23	1.901(9)	Te3–O29	1.923(9)	Te4–O35	1.903(7)
Te1–O18	1.908(9)	Te2–O24	1.911(8)	Te3–O30	1.925(8)	Te4–O36	1.917(9)
Te1–O19	1.930(9)	Te2–O25	1.912(8)	Te3–O31	1.926(9)	Te4–O37	1.926(9)
Te1–O20	1.934(9)	Te2–O26	1.918(9)	Te3–O32	1.928(8)	Te4–O38	1.938(8)
Te1–O21	1.943(9)	Te2–O27	1.922(9)	Te3–O33	1.956(9)	Te4–O39	1.938(8)
Te1–O22	2.016(9)	Te2–O28	1.998(9)	Te3–O34	1.962(9)	Te4–O40	1.957(9)
<Te1–O>	1.939	<Te2–O>	1.927	<Te3–O>	1.937	<Te4–O>	1.930
S1–O1	1.458(10)	S2–O5	1.461(10)	S3–O9	1.478(11)	S4–O13	1.463(10)
S1–O2	1.473(9)	S2–O6	1.471(11)	S3–O10	1.482(10)	S4–O14	1.470(10)
S1–O3	1.474(9)	S2–O7	1.480(10)	S3–O11	1.483(9)	S4–O15	1.473(10)
S1–O4	1.483(11)	S2–O8	1.488(12)	S3–O12	1.493(11)	S4–O16	1.482(12)
<S1–O>	1.472	<S2–O>	1.475	<S3–O>	1.484	<S4–O>	1.472
Hydrogen bonds							
O22···O8	2.853(16)	O41···O15	2.861(14)	O43···O8	2.729(15)	O44···O7	2.710(15)
O28···O10	2.833(13)	O42···O2	2.873(14)	O43···O38	3.040(13)	O44···O10	2.714(14)

axes was used to randomiSe the sample and observed *d* values and intensities were derived by profile fitting using *JADE Pro* software (Materials Data, Inc.). The powder data are presented in Supplementary Table S1 (see below).

Single-crystal X-ray studies were carried out on a Bruker APEX2 CCD diffractometer equipped with Mo*K*α radiation. The intensity data of flaggite were extracted from a crystal twinned by 180° rotation on [001]. All data were processed using Bruker *TWINABS*. The crystal structure was solved and refined in space group *P*1 using *SHELX* (Sheldrick, 2015a, 2015b). The refinement using the data from a single component was better than that using both components, so the single-component refinement is reported here. The limited data set, imperfect absorption correction and problems in separating the twinned data compromised the quality of the data resulting in large residual electron densities and problems with anisotropic displacement parameters. Consequently, the non-sulfate O atoms (O17–O44) could only be refined isotropically and several of the Cu, Te and sulfate O atoms, which were refined anisotropically, exhibited markedly prolate or oblate ellipsoids. Data

https://doi.org/10.1180/mgm.2022.37 Published online by Cambridge University Press

Table 5. Bond-valence sums for flaggite*. Values are expressed in valence units.

	Pb1	Pb2	Pb3	Pb4	Pb5	Pb6	Pb7	Pb8	Cu1	Cu2	Cu3	Cu4	Cu5	Cu6	Cu7	Cu8	Te1	Te2	Te3	Te4	S1	S2	S3	S4	H bonds	Sum	Assign.
O1	0.18					0.33															1.59					2.10	O
O2		0.10			0.29																1.53				0.16	2.08	O
O3	0.08	0.24								0.19											1.53					2.04	O
O4			0.24	0.26																	1.49					1.99	O
O5	0.18	0.21									0.11											1.58				2.08	O
O6							0.10	0.28														1.54				1.92	O
O7	0.12					0.14																1.50			0.22	1.98	O
O8		0.07			0.11																	1.47			0.17,0.21	1.65	O
O9							0.15	0.12															1.51			1.78	O
O10			0.11	0.07																			1.50		0.17,0.22	2.07	O
O11				0.17				0.18					0.14										1.49			1.98	O
O12	0.32					0.10																	1.46			1.88	O
O13							0.34	0.19																1.57		2.10	O
O14				0.24				0.09							0.16									1.54		2.03	O
O15			0.30	0.09																				1.53	0.16	2.08	O
O16		0.19			0.28																			1.50		1.97	O
O17						0.29			0.43	0.12							1.03									1.87	O
O18	0.13			0.30						0.38							1.02									1.83	O
O19	0.04				0.09						0.43			0.50			0.98									2.04	O
O20								0.34			0.47	0.19					0.98									1.98	O
O21				0.29					0.34				0.50				0.96									2.09	O
O22					0.05		0.14					0.24					0.84								–0.17	1.10	OH
O23	0.26			0.13									0.35					1.04								1.78	O
O24							0.28						0.13	0.44				1.02								1.87	O
O25		0.30													0.41	0.25		1.02								1.98	O
O26			0.09						0.47						0.44			1.01								2.01	O
O27	0.24									0.48				0.36				1.00								2.08	O
O28			0.05			0.14										0.24		0.87							–0.17	1.13	OH
O29		0.17						0.23			0.42								1.00							1.82	O
O30					0.41						0.13	0.44							0.99							1.97	O
O31			0.05					0.29				0.25			0.49				0.99							2.07	O
O32				0.43					0.10	0.49									0.99							2.01	O
O33			0.18			0.35			0.39										0.94							1.86	O
O34						0.28				0.39						0.48			0.93							2.08	O
O35	0.43												0.50	0.08						1.03						2.04	O
O36		0.34			0.04						0.48					0.23				1.01						2.10	O
O37		0.25						0.18							0.42					0.99						1.84	O
O38					0.18		0.32							0.40						0.97					0.12	1.99	O
O39			0.41												0.13	0.44				0.97						1.95	O
O40							0.25	0.04				0.48	0.39							0.94						2.10	O
O41					0.58	0.28										0.44									–0.16	1.14	OH
O42			0.60				0.30					0.36													–0.16	1.10	OH
O43					0.05	0.11								0.22											–0.21,–0.12	0.05	H_2O
O44			0.05				0.12		0.22																–0.22,–0.22	–0.05	H_2O
Sum	1.98	1.87	2.08	1.98	2.08	2.02	2.00	1.94	1.95	2.05	2.04	1.96	2.01	2.00	2.05	2.08	5.81	5.96	5.84	5.91	6.14	6.09	5.96	6.14			

* Te^{6+}–O bond valence parameters are from Mills and Christy (2013). All others are from Gagné and Hawthorne (2015). Hydrogen-bond strengths are based on O–O bond lengths from Ferraris and Ivaldi (1988). Negative values indicate donated hydrogen-bond valences.

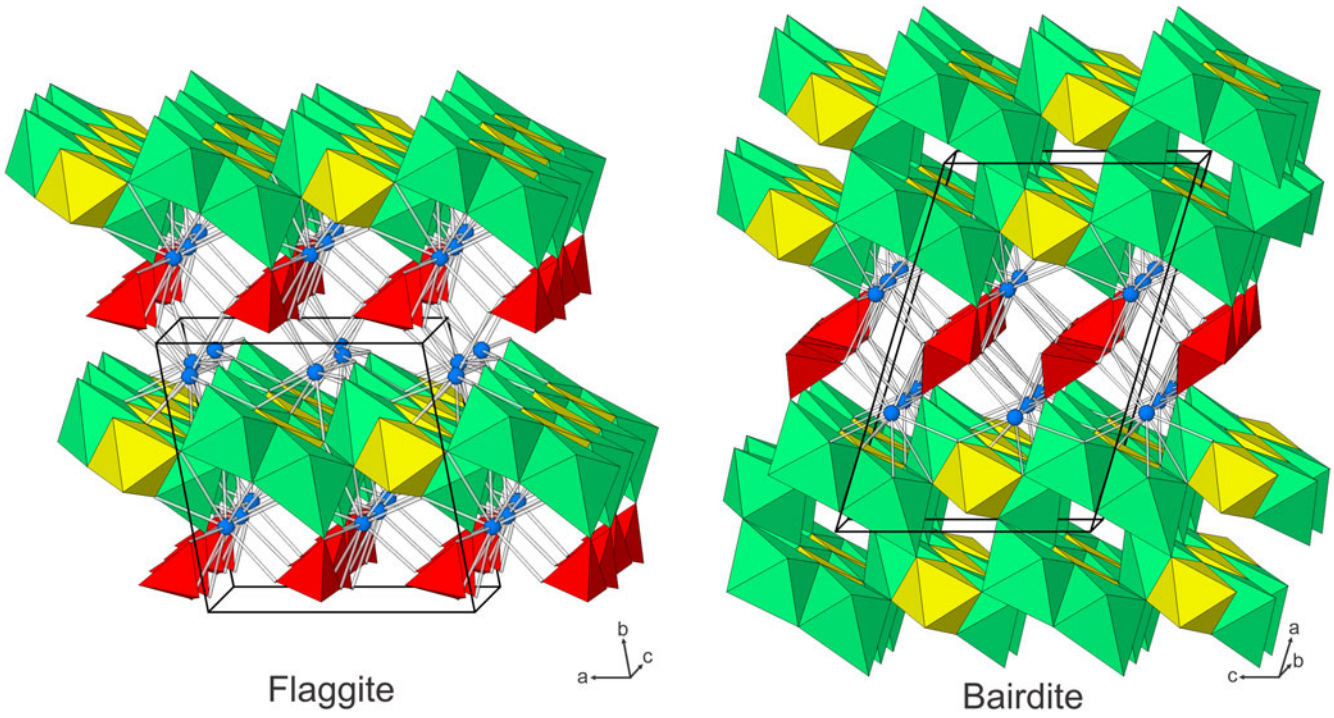

Fig. 4. The structures of flaggite and bairdite. Pb atoms are blue, SO_4 tetrahedra are red, TeO_6 octahedra are yellow, CuO_6 octahedra are green. The unit cell outlines are shown with thick black lines.

collection and refinement details are given in Table 2, atom coordinates and displacement parameters in Table 3, selected interatomic distances in Table 4 and bond-valence sums (BVS) in Table 5. The crystallographic information file (cif) has been deposited with the Principal Editor of *Mineralogical Magazine* and is available as Supplementary material. Note that the processing of the twinned structure data required merging of equivalent reflections prior running *SHELX*. Consequently, there is no R_{int} listed in the deposited cif. The number of reflections before merging and the R_{int} have been included in Table 2.

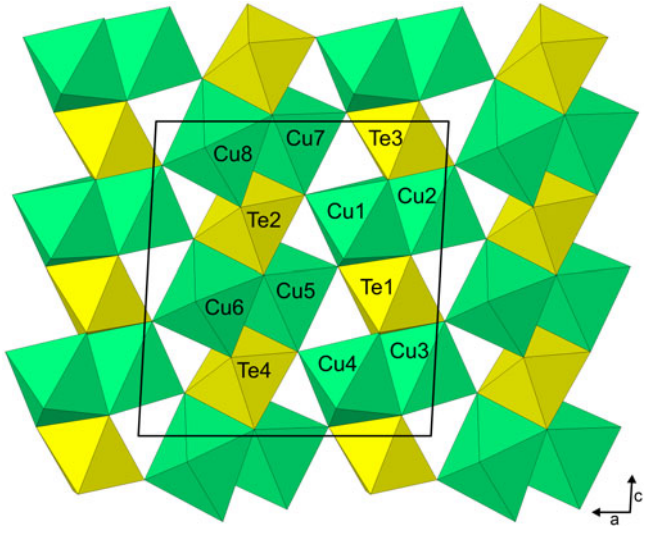

Fig. 5. Stair-step-like layer of edge-sharing TeO_6 and CuO_6 octahedra in the structure of flaggite. The unit cell outline is shown with thick black lines.

Description and discussion of the structure

In the structure of flaggite (Fig. 4), individual TeO_6 octahedra and pairs of edge-sharing Jahn-Teller distorted CuO_6 octahedra link by edge-sharing into chains along [001]. The chains are linked to one another by corner-sharing to form stair-step-like layers parallel to {010} (Fig. 5). The region between the layers contains SO_4 tetrahedra and Pb^{2+}. The SO_4 tetrahedra link by corner sharing to the apical O atoms of the CuO_6 octahedra projecting from only one side of the octahedral layer. The eight distinct Pb^{2+} atoms bond to either eight or nine O atoms. The Pb^{2+}–O bonds cover a broad range (2.274 to 3.451 Å); however, there are no pronounced lopsided distributions of bond lengths typical of Pb^{2+} with stereoactive $6s^2$ lone-pair electrons.

The same types of edge-sharing chains forming stair-step-like octahedral layers occur in the structures of bairdite, $Pb_2Cu_4^{2+}Te_2^{6+}O_{10}(OH)_2(SO_4)(H_2O)$ (Kampf *et al.*, 2013), timroseite, $Pb_2Cu_5^{2+}(Te^{6+}O_6)_2(OH)_2$ (Kampf *et al.*, 2010), and paratimroseite, $Pb_2Cu_4^{2+}(Te^{6+}O_6)_2(H_2O)_2$ (Kampf *et al.*, 2010). The structure is most similar to that of bairdite; however, there is a double stair-step layer in bairdite, as well as SO_4 groups projecting from both directions into the interlayer (Fig. 4), although it should be noted that the SO_4 groups in the bairdite structure are half-occupied. The flaggite structure can be derived from that of bairdite by removing one stair-step layer and the SO_4 groups projecting in one direction. An interesting feature of the stair-step-like layers in all of these structures is that they are based upon hexagonal close packing (HCP), not only in terms of the individual steps (or chains), but also with respect to the continuous assembly of steps. In the structural classification of Te oxycompounds of Christy *et al.* (2016b), flaggite has a structure with monomeric $Te^{6+}X_6$ as part of a larger structural unit that is an infinite layer.

https://doi.org/10.1180/mgm.2022.37 Published online by Cambridge University Press

Acknowledgements. Oleg Siidra, an anonymous reviewer and Structures Editor Peter Leverett are thanked for their constructive comments on the manuscript. A portion of this study was funded by the John Jago Trelawney Endowment to the Mineral Sciences Department of the Natural History Museum of Los Angeles County.

Supplementary material. To view supplementary material for this article, please visit https://doi.org/10.1180/mgm.2022.37

References

Christy A.G., Mills S.J., Kampf A.R., Housley R.M., Thorne B. and Marty J. (2016a) The relationship between mineral composition, crystal structure and paragenetic sequence: the case of secondary Te mineralization at the Bird Nest drift, Otto Mountain, California, USA. *Mineralogical Magazine*, **80**, 291–310.

Christy A.G., Mills S.J. and Kampf A.R. (2016b) A review of the structural architecture of tellurium oxycompounds. *Mineralogical Magazine*, **80**, 415–545.

Ferraris G. and Ivaldi G. (1988) Bond valence vs. bond length in O···O hydrogen bonds. *Acta Crystallographica*, **B44**, 341–344.

Gagné O.C. and Hawthorne F.C (2015) Comprehensive derivation of bond-valence parameters for ion pairs involving oxygen. *Acta Crystallographica*, **B71**, 562–578.

Gunter M.E., Bandli B.R., Bloss F.D., Evans S.H., Su S.C. and Weaver R. (2004) Results from a McCrone spindle stage short course, a new version of EXCALIBR, and how to build a spindle stage. *The Microscope*, **52**, 23–39.

Kampf A.R., Mills S.J., Housley R.M., Marty J. and Thorne B. (2010) Lead-tellurium oxysalts from Otto Mountain near Baker, California: V. Timroseite, $Pb_2Cu_5^{2+}(Te^{6+}O_6)_2(OH)_2$, and paratimroseite, $Pb_2Cu_4^{2+}(Te^{6+}O_6)_2(H_2O)_2$, new minerals with edge-sharing Cu–Te octahedral chains. *American Mineralogist*, **95**, 1560–1568.

Kampf A.R., Mills S.J., Housley R.M., Rossman G.R., Marty J. and Thorne B. (2013) Lead–tellurium oxysalts from Otto Mountain near Baker, California: X. Bairdite, $Pb_2Cu_4^{2+}Te_2^{6+}O_{10}(OH)_2(SO_4)\cdot H_2O$, a new mineral with thick HCP layers. *American Mineralogist*, **98**, 1315–1321.

Kampf A.R., Mills S.J., Celestian A.J., Ma C., Yang H. and Thorne B. (2021a) Flaggite, IMA 2021-044. CNMNC Newsletter 63. *Mineralogical Magazine*, **85**, 910–915, https://doi.org/10.1180/mgm.2021.74.

Kampf A.R., Mills S.J., Housley R.M., Ma C. and Thorne B. (2021b) Tombstoneite, IMA 2021–053. CNMNC Newsletter 63; *Mineralogical Magazine*, **85**, 910–915, https://doi.org/10.1180/mgm.2021.74.

Mandarino J.A. (2007) The Gladstone–Dale compatibility of minerals and its use in selecting mineral species for further study. *The Canadian Mineralogist*, **45**, 1307–1324.

Mills S.J. and Christy A.G. (2013) Revised values of the bond valence parameters for Te^{IV}–O, Te^{VI}–O and Te^{IV}–Cl. *Acta Crystallographica*, **B69**, 145–149.

Mills S.J., Kampf A.R., Christy A.G., Housley R.M., Rossman G.R., Reynolds R.E. and Marty J. (2014) Bluebellite and mojaveite, two new minerals from the central Mojave Desert, California, USA. *Mineralogical Magazine*, **78**, 1325–1340.

Missen O.P., Ram R., Mills S.J., Etschmann B., Reith F., Shuster J., Smith D.J. and Brugger J. (2020) Love is in the Earth: a review of tellurium (bio)geochemistry in surface environments. *Earth-Science Reviews*, **204**, 103150.

Missen O.P., Etschmann B., Mills S.J., Sanyal S.K., Ram R., Shuster J., Rea M.A.D., Raudsepp M.J., Fang X.-Y., Lausberg E.R., Melchiorre E., Dodsworth J., Liu Y., Wilson S.A. and Brugger J. (2022a) Tellurium biogeochemical transformation and cycling in a metalliferous semi-arid environment. *Geochimica et Cosmochimica Acta*, **321**, 265–292, https://doi.org/10.1016/j.gca.2021.12.024.

Missen O.P., Mills S.J., Rumsey M.S., Spratt J., Najorka J., Kampf A.R. and Thorne B. (2022b) The new mineral tomiolloite, $Al_{12}(Te^{4+}O_3)_5[(SO_3)_{0.5}(SO_4)_{0.5}](OH)_{24}$: a unique microporous tellurite structure. *American Mineralogist*, **107**, https://doi.org/10.2138/am-2022-8368.

Sheldrick G.M. (2015a) SHELXT – Integrated space-group and crystal-structure determination. *Acta Crystallographica*, **A71**, 3–8.

Sheldrick G.M. (2015b) Crystal structure refinement with SHELXL. *Acta Crystallographica*, **C71**, 3–8.

Williams S.A. (1980) The Tombstone district, Cochise County, Arizona. *Mineralogical Record*, **11**, 251–256.